OPTICAL SPECTROSCOPY OF LATERALLY SPACED InAs/GaAs QUANTUM DOT MOLECULES

by

Shilpa Sanwlani

A thesis submitted to the Faculty of the University of Delaware in partial fulfillment of the requirements for the degree of Master of Materials Science and Engineering

Winter 2010

OPTICAL SPECTROSCOPY OF LATERALLY SPACED
InAs/GaAs QUANTUM DOT MOLECULES

by

Shilpa Sanwlani

Approved:

Matthew F. Doty, PhD.
Professor in charge of the thesis

Approved:

David Martin , PhD.
Chair of the Department of Materials Science and Engineering

Approved:

Michael J. Chajes, PhD.
Dean of College of Engineering

Approved:

Debra Hess Norris, M.S.
Vice Provost for Graduate and Professional Education

ACKNOWLEDGEMENT

This work would have not been successfully completed without the unsparing and conscientious help of some very important persons. First and foremost, I wish to express my sincere gratitude to my advisor, Dr. Mathew F. Doty, for his invaluable academic guidance and unfailing moral support. He was always there to listen and advise me. He showed me different ways to approach a research problem and the need to be persistent to accomplish any goal. I would also like to thank my colleagues, Weiwen Liu, Will Reid, Xinran Zhou and Chelsea Haughn for their support throughout the project and for making DuPont Lab 203 a great place to work.

I would also like to thank our collaborators, Dan Gammon (NRL), Allan Bracker (NRL), Greg Salamo (University of Arkansas) and Jihoon Lee (Kwangwoon University, South Korea) for growing the materials that were studied in this work.

I cannot acknowledge my parents, Lt Baldev Raj Sanwlani and Mamta Sanwlani, and my sisters, Prerna, Sheetal, Preeti enough. Their love, support and encouragement provided comfort and assurance at all times. They, along with Amandeep Arora, have been my pillars of strength through this journey.

Contents

List of Figures

List of Tables

ABSTRACT

Over the past decade, potential device applications have fueled an extensive effort to fabricate lateral arrays of quantum dots (QDs) with specific dot densities, spacings and size distributions. An essential element for the further development of QD devices with new functionalities is the introduction of controllable quantum coupling between two or more QDs in such an array. Tunable quantum coupling between vertically stacked InAs QDs has been demonstrated, with the coupling mediated by coherent tunneling and tunable with a static electric field. While these studies have revealed that the spatial arrangement of QDs can lead to remarkable effects, it will be impossible to scale vertical coupling to a large number of QDs. Investigations of lateral quantum coupling have been slower to develop, however, because special growth protocols are required and the ability to independently tune the luminescence energy of separate QDs is lost.

Spectroscopy of single pairs of laterally separated QDs is required to resolve the signatures of quantum coupling from inhomogeneously broadened ensemble spectra. Laterally-coupled quantum dots require modified sample preparation methods to isolate single pairs of QDs and apply electric fields that tune the relative energies of the two dots.

The electric field must be applied along the surface of the sample, perpendicular to the growth direction. To apply this lateral field, we use interdigitated electrodes patterned onto the sample surface with photolithography and metal deposition. Electrical connections are made to each of the interdigitated top contacts as well as to an ohmic back contact. This three-terminal arrangement makes it possible to independently control both the relative energies of the dots and the charging of the QDs. We present photoluminescence spectra of laterally coupled QDs whose coupling and charge states are tuned with this three-terminal arrangement. We further discuss the implications and opportunities for control of quantum coupling in laterally-scalable architectures.

LIST OF SYMBOLS

Ψ	Wavefunction
α, β	Probability Amplitudes
s,p,d,f	Orbital Energy Levels
$\hbar$	Reduced Planck's constant
m^*	Effective Mass
∇	Gradient
$V(r)$	Confinement Potential
$F_k(r)$	Average Envelope Wavefunction
$\in$	Electron Energy
$r(x, y, z)$	Electron Position Vector
$\phi(r)$	Normalized Wavefunction of Electron
Ω	Unit Cell Volume
$u_0(r)$	Bloch function normalized in the unit cell
$V(x)$	Confinement Potential in the x direction
$V(y)$	Confinement Potential in the y direction
$V(z)$	Confinement Potential in the z direction
L_x	Length of confined region in x direction
L_y	Length of confined region in y direction
L_z	Length of confined region in z direction

D(E)	Density of states
N$_D$	Volume density of quantum dots
a$_I nAs$	Lattice constant of InAs
a$_G aAs$	Lattice constant of GaAs
$\in_{x\ x}$	Uniaxial strain in x direction
$\in_{y\ y}$	Uniaxial strain in y direction

LIST OF ACRONYMS

QIP	Quantum Information Processing
QD	Quantum Dot
NV	Nitrogen Vacancy
QDM	Quantum Dot Molecule
PL	Photoluminescence
FM	Frank-van der Merwe
VW	Volmer Weber
SK	Stranski-Krastanov
III-V	Three-five compound semiconductor
MBE	Molecular Beam Epitaxy
CB	Conduction Band
V_B	External Bias Voltage
E_F	Fermi Energy
X^0	Neutral Exciton
X^+1	Positive trion
X^-1	Negative trion
X^-2	Doubly Negative Charged Exciton
NIR	Near Infrared
PLE	Photoluminescence

Chapter 1

Introduction

1.1 Introduction to Spintronics

Conventional electronic devices rely on the transport of electrical charge carriers, electrons, in a semiconductor such as silicon. However, researchers are trying to exploit the 'spin' of the electron rather than its charge to create a remarkable new generation of 'spintronic' devices that will be smaller, faster and more versatile than today's devices.

The spin of a single electron provides a natural two-level system (up or down) that is suitable for use as a bit, the fundamental logical unit [1]. The future potential of spin electronics in the field of information storage and ultimately quantum computing has been long recognized. Experiments to explore the transfer of spin-polarized electric current in small devices have been ongoing for 30 years.

However, attaining precise control over the transport of spins in micro-scale and nano-scale devices remains elusive. A discovery by Awschalom and Kikkawa in 1999 [2] rekindled interest in the utility of semiconductors for spin based devices. They demonstrated that optically injected spin-polarized carriers maintain their coherence over nanosecond time scales. This result demonstrated that spins can be transported over distances of tens of micrometers, enabling the transport of coherent spin information from point to point within a device. This result was instrumental in understanding the coherent evolution of spin states in semiconductors for the spintronics and quantum information processing (QIP) research.

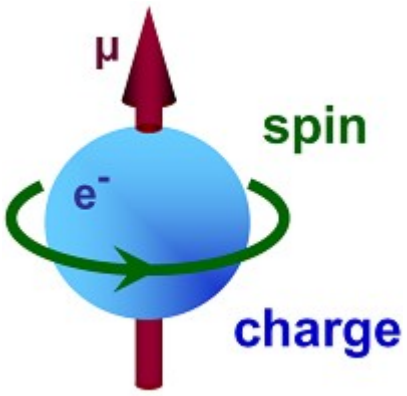

Figure 1.1: Schematic of spin of an electron

The spins can, for example, form the basis of an optical memory in which selective addressing of individual spins in both wavelength and spatial domains may be utilized to increase the ultimate information storage density achievable [5]. There are many spin-based proposals for both spintronics and quantum in-

formation processing (QIP). The two spin projections are proposed as bit states. The difference is whether they are manipulated coherently. If the spin bit can be coherently controlled, it can be used as a qubit, the fundamental logical unit for quantum information processing (or quantum computing). In QIP the information is not encoded in just the spin projection but also the quantum phase, which necessitates the coherent control. The term quantum computing includes all methods to devise and implement coherent logic operations for computation and communication.

A qubit (or quantum bit)is the analog of a bit for quantum computation. An ordinary bit assumes only two possible values (usually called 0 and 1), a qubit may assume a continuum of values. A pure qubit state is a linear superposition of those two states. This means that the qubit can be represented as a linear combination of $|0\rangle$ and $|1\rangle$:

$$|\psi\rangle \quad = \quad \alpha\,|0\rangle + \beta\,|1\rangle \tag{1.1}$$

[3]

where α and β are probability amplitudes satisfying

$$|\alpha|^2 + |\beta|^2 = 1 \tag{1.2}$$

An important distinguishing feature between a qubit and a classical bit is that

multiple qubits can exhibit quantum entanglement. Entanglement is a nonlocal property that allows a set of qubits to express higher correlation than is possible in classical systems. Take, for example, two entangled qubits:

$$\frac{1}{\sqrt{2}}\left(|0\rangle + |1\rangle\right) \tag{1.3}$$

In this state, called an equal superposition, there are equal probabilities of measuring either $|0\rangle$ or $|1\rangle$, as

$$\left(\frac{1}{\sqrt{2}}\right)^2 = \frac{1}{2} \tag{1.4}$$

Taken together, quantum superposition and entanglement create an enormously enhanced computing power. Where a 2-bit register in an ordinary computer can store only one of four binary configurations (00, 01, 10, or 11) at any given time, a 2-qubit register in a quantum computer can store all four numbers simultaneously, because each qubit can be in superposition of two values. If more qubits are added, the increased capacity is expanded exponentially i.e. the number of states that can be entangled in a quantum computer is 2^n, where n is the number of qubits used.

Semiconductor quantum dots (QDs) in which carriers are confined in all the three dimensions are attractive candidates for spin based logic operations. The

discrete energy levels of the QD allow a discrete number of charges to be localized with well-defined spin projections. Information can be stored in the value of the spin of the charge carriers confined in the QDs. It is possible to prepare the spin in a precisely defined state and make it persist long enough to allow its manipulation. For spin-based logic operations, spin lifetime is the limiting factor. Lifetimes up to 1 sec at low magnetic field [7] have been observed for spins confined in QDs. The primary mechanism that leads to spin relaxation in bulk semiconductors has been identified theoretically as the spin-orbit interaction that weakly couples the spin and charge degrees of freedom of the electron [4]. Because the electron charge is coupled to the lattice vibrations (phonons) in the host crystal, the spin-orbit interaction permits the lattice vibrations to act as a dissipative environment for the spin. This mechanism is strongly suppressed in confined electron states of a QD. If the spin-based logic operations can be realized coherently, spins in QD can become a tool for implementing quantum information processing. For both spintronics and quantum information processing, the need is to have systems in which single spins can be isolated and controlled, preferably coherently. QDs are particularly interesting because they can localize single spins can be accessed and manipulated optically.

1.2 Materials for implementation of quantum logic operations

There are several physical systems in which one could realize coherent logic operations.In iontrap systems,a variety of quantum operations and algorithms have been performed using discrete energy levels of the ions coupled by the quantized motion of the ions (phonons) [8].In cavity quantum electrodynamics experiments, quantum computations at the level of two qubit gates have been demonstrated. However, it is unclear whether these atomic physics implementations could be scaled to large scale quantum operations [9]. Another possible material for quantum logic is the superconducting qubit made from one or more Josephson junctions. The advantage of superconducting qubits is their strong coupling to microwave signals, which can control the qubits and mediate their interactions [6]. The limitation is that the superconducting systems have short coherence lifetime and they do not permit the use of ultrafast optics which QD based systems allow.

Optical approaches to manipulating quantum coherence enable rapid gate operations by the use of ultrafast lasers.In quantum-optics,single qubit operations have been performed using cold trapped ions, localizing electron spins around isolated nitrogen-vacancy (NV) centers in diamond [10]and using an electron spin trapped in semiconductor quantum dots (QDs). The key step is to develop a method for reliable spin-state manipulation with sufficiently long spin coherence

times. NV centers in diamond are quite promising because they have long spin coherence times and can be coherently manipulated at room temperature. QDs typically require low temperatures due to their comparatively weak orbital quantization energies. On the other hand, arrays of self assembled QDs can be readily formed, making them potentially more scalable. Unlike lithographically defined QDs, self assembled QDs confine both electrons and holes simultaneously, and thus are optically active. This allows the spin state of confined charges to be optically manipulated and interrogated.

The ability to coherently initialize, control and read out a two level quantum state is an essential requirement for any quantum information protocol. In the case of spin-based logic, maintaining coherence requires that the quantum phase in a superposition of spin states be preserved. Due to the interaction of the spin with the environment both the spin projection and the phase tend to decay with characteristic times, the spin relaxation and the spin decoherence times respectively. A primary source of decoherence is the hyperfine interaction of an electron with the millions of nuclear spins present in a QD. Using hole spins to store information may be one of solution to this problem because the valence band origin of hole states eliminates the contact hyperfine interaction, strongly suppressing the primary decoherence mechanisms. In this work we will be exploring pairs of coupled QDs as possible materials for confining and controlling single spins for applications in both spintronic and quantum information processing devices.

1.3 Overview of the thesis

This thesis is divided into three chapters. The second chapter describes the basic theoretical background on QDs as a revolutionary step in the research field of zero-dimensional nanostructures. The epitaxial growth technique used to synthesize the QDMs is discussed, along with a brief summary of the other epitaxial growth modes of semiconductor heterostructure. It presents an overview of the Optical Spectroscopy of Single Quantum Dot (QD) and quantum dot molecules (QDMs)

Chapter 3 deals with an overview of time integrated photoluminescence(PL) spectroscopy used to study the optoelectronic properties of QDs and QDMs. The experimental study to understand the spin charge interactions in single QD and coupling in vertically coupled InAs/GaAs QDMs is presented. Optical properties of dots and molecules are studied using PL spectroscopy with varying electric field. Preliminary results for the coupling in lateral InAs/GaAs QDMs is presented.In the end it concludes with summarizing the experimental work presented in this thesis. Future work that can provide further and deeper understanding of coupling in Lateral QDMs is proposed.

Chapter 2

Electronic properties of InGaAs quantum dots

In this section, I will use an elementary quantum-mechanical approach to survey how the energy levels, wave functions, and density of states of charge carriers confined in the dot depend on the dimension of the quantum dots. I will then describe the methods used to fabricate the types of quantum dots we investigate and reciew the methods used to prepare our samples. Finally I will describe the optical spectroscopy methods used to characterize charge and spin interactions in coupled quantum dots.

2.1 Background on Quantum Dot Molecules

When the size of a semiconductor crystal is reduced to the nanometer scale in one direction and that crystal is surrounded by another semiconductor material that acts as a potential barriers, the freedom of electron movement is lost in that direction. The potential height corresponds to the band offset between the two crystals in the conduction and valence bands. Electrons in the bulk material move in all directions; in a quantum well they move in the x-y plane; in a quantum wire they move in the x direction. QDs have electrons confined to the physical dimensions comparable to de Broglie wavelength, in all three dimensions. As a result the energy levels are fully quantized. QDs are often called artificial atoms because they locally confine single charges in discrete energy states analogous to orbital energy levels (s,p,d etc) of natural atoms.

This confinement also results in changes to the electron density of states. The control over discrete energy levels and density of states are two of the the most remarkable and significant benefits of low-dimensional semiconductor technology [11]. The tunability of these properties with nanostructure parameters overcomes the lack of versatility in traditional semiconductors.

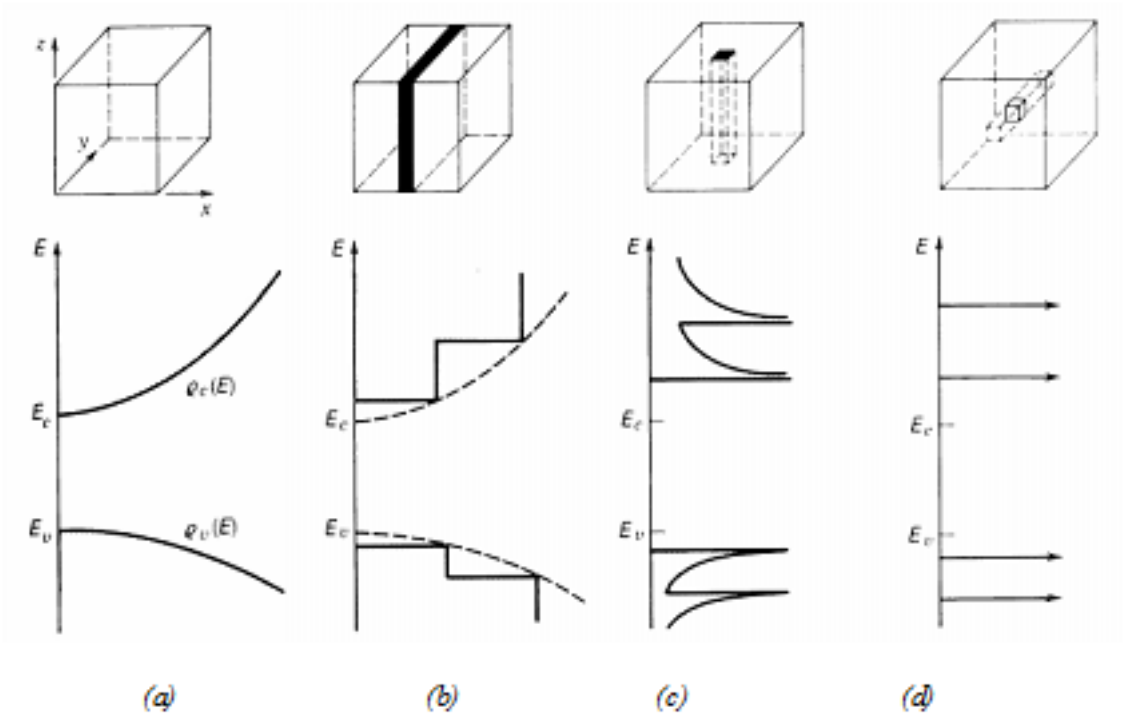

Figure 2.1: Comparison of the quantization of density of states: (a) bulk, (b) quantum well, (c) quantum wire, (d) quantum dot [11].

2.1.1 Quantum Dots

The band-edge electron states of semiconductors can be described by the effective-mass equation as

$$\left[-\frac{\hbar^2}{2m^*}\nabla^2 + V\left(r\right)\right] F_K\left(r\right) = \in F_K\left(r\right) \tag{2.1}$$

Here, m^* is the effective mass; $\hbar$ is Planck's constant divided by 2π; r(x, y, z) is the electron position vector; V(r) is the confinement potential. F$_K(r)$ is the average envelope wave function, and $\in$ is the electron energy [11]. The normalized wave function for an electron close to the band edge is written simply as

$$\Phi\left(r\right) = \sqrt{\Omega} F_K\left(r\right) u_0\left(r\right) \tag{2.2}$$

where Ω is the unit cell volume and $u_0\left(r\right)$ is the Bloch function normalized in the unit cell, Assuming an infinitely high confining potential in all directions, the confinement potential becomes V((r) = V(x) + V(y) + V(z). Thus, we get

$$\in = E\left(k\right) = \frac{\hbar^2 k^{\|2}}{2m^*} + E_{nx} + E_{ny} + E_{nz} \tag{2.3}$$

$$= \frac{\hbar^2}{2m^*}\left[\left(\frac{n_x\pi}{L_x}\right)^2 + \left(\frac{n_y\pi}{L_y}\right)^2 + \left(\frac{n_z\pi}{L_z}\right)^2\right] \tag{2.4}$$

where n_x, n_y, n_z = 1,2,3, etc., L_x, L_y, and L_z are the lengths of the confined region in each direction and k = $\left(\frac{n_x\pi}{L_x}, \frac{n_y\pi}{L_y}, \frac{n_z\pi}{L_z}\right)$. The most important consequence of the confinement is that the energy states are quantized into discrete states that are indexed by the integers n. The corresponding wave function is

$$F_K(r) = \Phi_{nx}(x) + \Phi_{ny}(y) + \Phi_{nz}(z) \tag{2.5}$$

As a result of the quantized energy levels, the density of states is a series of delta function. Assuming that all quantum dots in a sample are identical, the density of states can be written as

$$D(E) = 2N_D \sum \delta \lfloor E - E_{nx} - E_{ny} - E_{nz} \rfloor \tag{2.6}$$

where N_D is the volume density of quantum dots, and the factor of two presents the degeneracy due to spin.

2.1.2 InAs/GaAs Quantum Dots

In the preceding section we showed that a strong confining potential leads to discrete energy states analogous to the particle-in-a-box model from elementary quantum mechanics. The task remains to implement such confining potentials experimentally. In the 1990s a modified Stranski-Krastanov growth mechanism

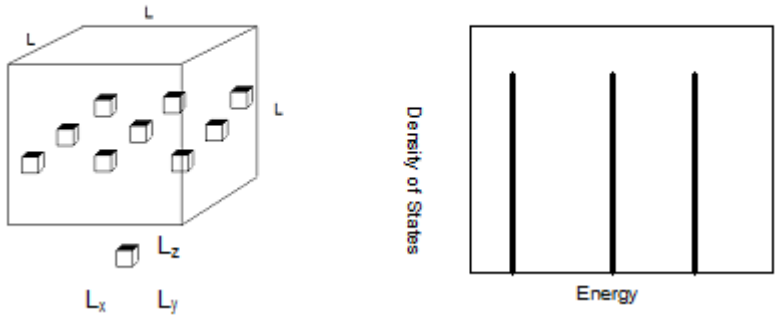

Figure 2.2: Schematic view and graph of quantum dot and its density of states [11]

driven by self-organization phenomena at the surface of strongly strained heterostructure was developed to fabricate such dots. This growth process presents a sound way to easily and quickly fabricate large numbers of quantum dots. A rapidly increasing number of laboratories around the world have embarked on investigation and modeling of the growth, physical properties, and device applications of the numerous possible material combinations that can be used to form quantum dots in this manner.

As depicted in Fig. 2.3, there are three different growth modes that can occur when one material is epitaxially deposited on a substrate with different material composition. In Frank-van der Merwe (FM) mode, growth proceeds layer by layer. In Volmer-Weber (VW) mode the deposited film has a higher surface energy than that of the substrate, which causes the formation of three-dimensional islands

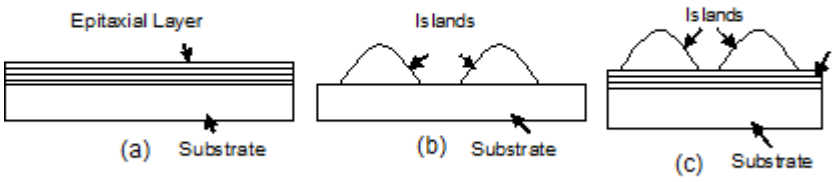

Figure 2.3: Three epitaxial growth modes on a substrate: (a) Frank-van der Merwe (FM), (b) Volmer-Weber (VW), and (c) Stranski-Krastanov (SK)

on the substrate. Stranski-Krastanov (SK) growth is a combination of FM and VW modes in which the growth of a several-monolayer thin film, called a wetting layer, is followed by cluster nucleation and then by island formation. The growth mode that occurs depends primarily on the difference in the surface energy between the substrate and the growth material and on the strain energy accumulated in the growth materials as a result of lattice mismatch.

The quantum dot heterostructure studied in this thesis are III-V materials consisting of InAs grown on a GaAs [100] substrate by molecular beam epitaxy (MBE). This material combination meets the criteria for Stranski-Krastanov growth. First, the lattice constant of the depositing layer and substrate are different, which permits strained layer heteroepitaxial growth to occur. The lattice constant for InAs is a_{InAs} = 6.056 and that for GaAs is a_{GaAs} = 5.653 . Second, the InAs is biaxially strained to make up for the lattice mismatch. The strain tensor

for the lattice mismatch defined by its in-plane components is given by:

$$\in_x = \in_y = \frac{aGaAs - aInAs}{aInAs} \tag{2.7}$$

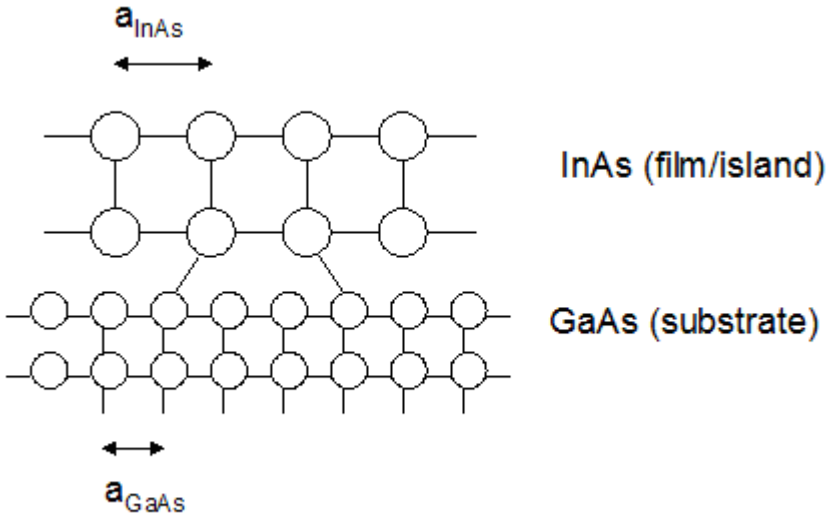

Figure 2.4: Lattice mismatch between InAs and GaAs

The lattice mismatch between InAs and GaAs is compressive, as the strain (-6.67 percent) is negative. This is illustrated in Fig 2.4. Thus the SK growth method permits the self-assembly of dislocation-free high density dots (islands) of InAs on GaAs substrates.

2.2 Spectroscopy of Quantum Dot (QD) and Quantum Dot Molecule (QDM)

To investigate coupled pairs of QDs as a material for the localization and control of single spins, we optically probe and electronically tune the quantum coupling between charges and spins confined in Quantum Dots. The devices investigated consist of InGaAs self-assembled QDs embedded within a GaAs n-i- Schottky diode structure, which allows for control of the total charge state of the dot and the relative energies between the two dots. To study interactions within a single QDM, the sample surface is covered with an aluminum mask containing 1μm apertures. This process of isolating single QDM is for vertical QDMs, the process for Lateral QDMs will be studied in next section.

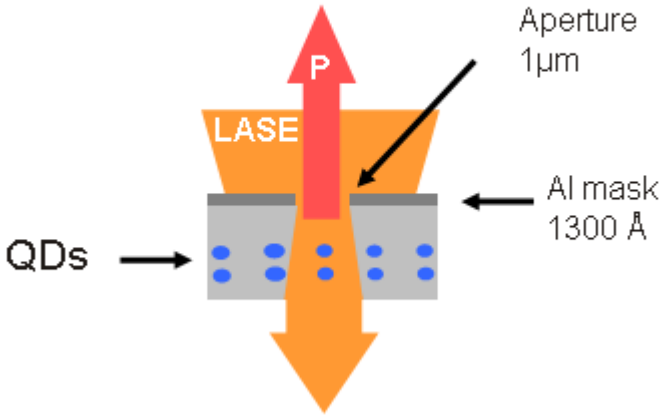

Figure 2.5: Isolate Single Quantum Dots

Our primary optical probe method is photoluminescence. The sample is illuminated with a continuous wave laser that excites an electron across the band gap, leaving behind a hole. The excited electron-hole pair relaxes into the low energy states of the QD. When the ground state for electrons and holes are populated by one carrier each, the electron and hole are bound to form an exciton. They recombine and emit a photon, whose energy tells us about the energy levels in the QDs.

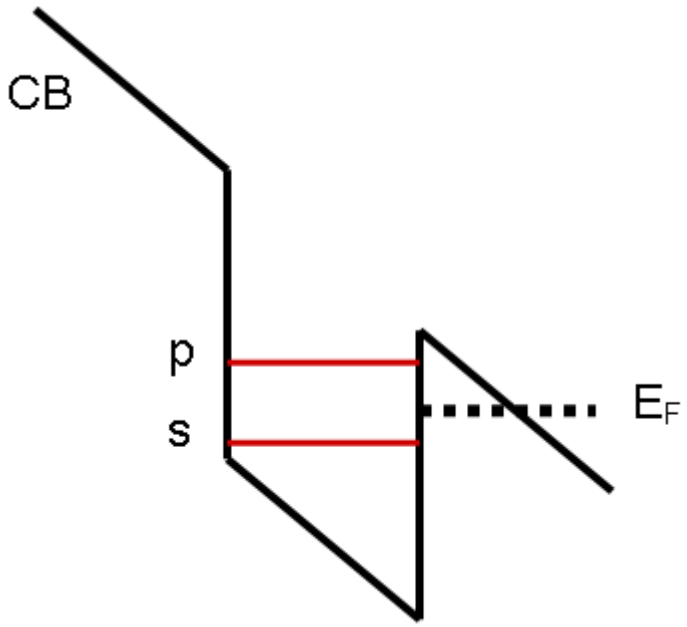

Figure 2.6: Energy-band structure of the QD with the applied electric field

The charge occupation of the QDs can be controlled by varying the external bias voltage V_B applied between a Schottky gate on the top surface and the back contact made to an n-doped substrate. For increasing V_B the band flattens and the

QD electron levels are subsequently shifted below the Fermi energy E_F of the n-GaAs region. This results in a step-by-step occupation of the QD with electrons. First, the QD s shell is brought below E_F. As a consequence the s shell is occupied with one electron via tunneling between the n-GaAs region and the QDs. The voltage for which the second s-shell electron state is occupied is larger. This is due to the fact that a Coulomb charging energy of about 20 meV has to be taken into account for the second electron [12]. No more than two electrons can occupy the s-shell due to the Pauli Exclusion Principle. There is thus a significant energy barrier to the occupation of the QD with three or more electrons and a larger applied bias is required to bring these levels below the Fermi level.

In a single quantum dot (QD), controlled single-electron charging allows us to identify neutral, single and double-charged excitons in the optical spectra [13]. The form of single dot data is well established, consisting of emission from a charge neutral exciton (X^0 = 1e + 1h) that is replaced by singly (X^-1 = 2e + 1h) and doubly (X^-2 = 3e + 1h) negatively charged transitions as the electric field reduces and electrons transfer into the dot from the adjacent n contact. Coulomb interactions between the charges introduce characteristic energy shifts for each charge state. For example, the observed spectral line for X^-1 is typically 3-6 meV below X^0.

A single dot can localize a single charge with freedom of the spin orientation, but the addition of further charges sacrifices the spin freedom because multiple

charges in the same energy level must have opposite spin projections. Thus a single QD is fundamentally limited to one or two qubit operations with little or no prospects of further scalability. As a result, attention has shifter towards few dot nanostructures, particularly vertically stacked quantum dot molecules (QDMs) that have potential for scalable and more complex quantum systems. Quantum Dot Molecule (QDM) spectra will be more complicated because there are more possible locations for the electron and hole, and more tuning of relative energy levels. The two dots forming a vertically-stacked QDM are separated by a spacer layer whose thickness determines the intrinsic strength of the tunnel coupling between the dots.

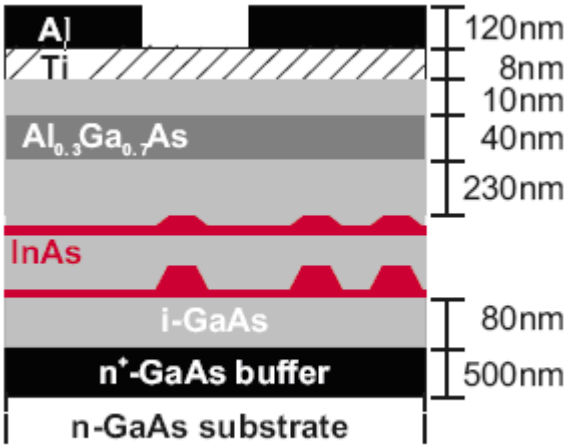

Figure 2.7: Schematic of the QDM sample structure [14]

The presence of charge carriers in both dots leads to two classes of excitonic recombination. One is when the electron and hole that recombine to emit a photon are located in the same dot; the resulting Photoluminescence (PL) line is called "direct" exciton. The other is "indirect" exciton where electrons and holes are located in the different dots. Direct excitons have a weak energy dependence on the applied electric field, whereas indirect excitons have a strong dependence on the applied electric field due to the spatial separation between the dots and consequent change in relative energy levels with the applied field. Direct and indirect excitons appear as horizontal and diagonal lines respectively in a spectral map which is a plot of PL intensities as a function of both applied electric field and energy.

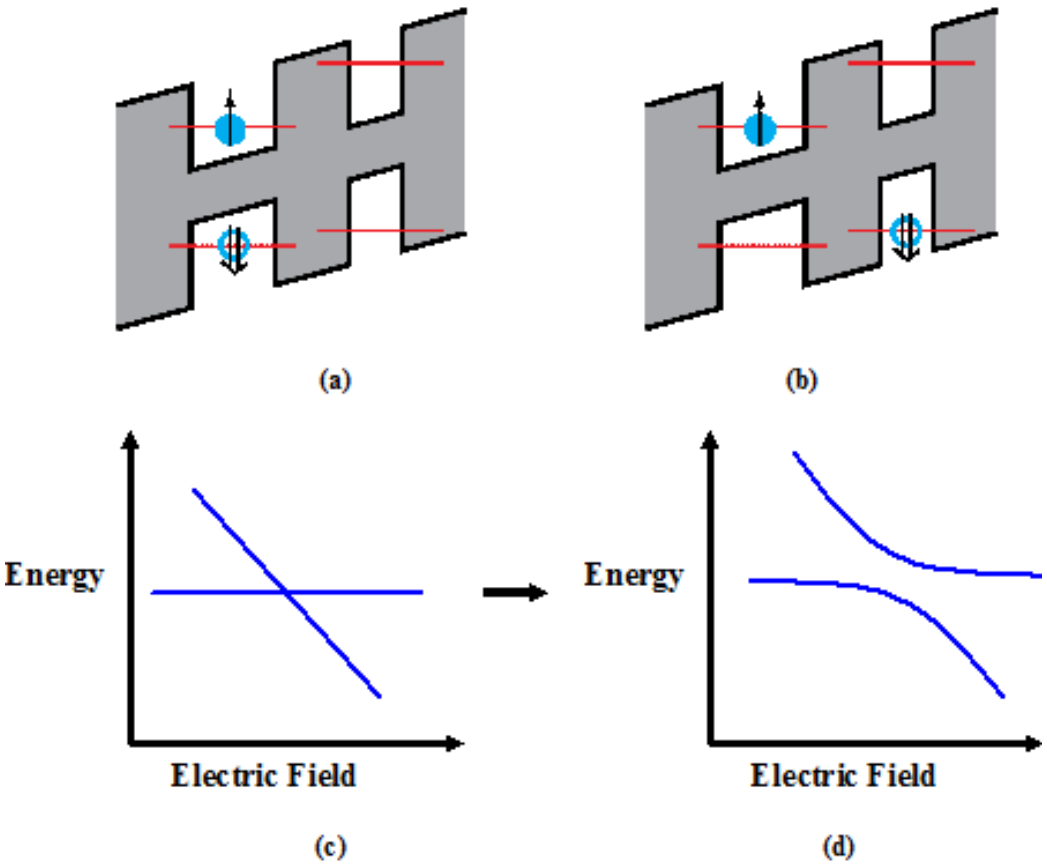

Figure 2.8: Schematic of electron and hole in the (a) same dot and in the (b) different dot. (c) Direct and indirect excitons cross at resonant energy which gives rise to (d) an anticrossing

Direct and indirect exciton PL lines would cross at an applied electric field that brings the energy levels of the two dots into resonance. When the applied electric field tunes electron or hole energy levels into resonance, the electrons or holes can tunnel between the two dots. Tunneling couples the states of the two dots and results into the formation of molecular orbitals delocalized over both the dots. The formation of molecular orbitals results in avoided crossings (anticrossings) between direct and indirect excitons as a function of applied electric field. At the anticrossings, the orbital wave functions of the exciton take on "bonding" and "antibonding" characters analogous to the molecular orbitals in diatomic molecules [15].

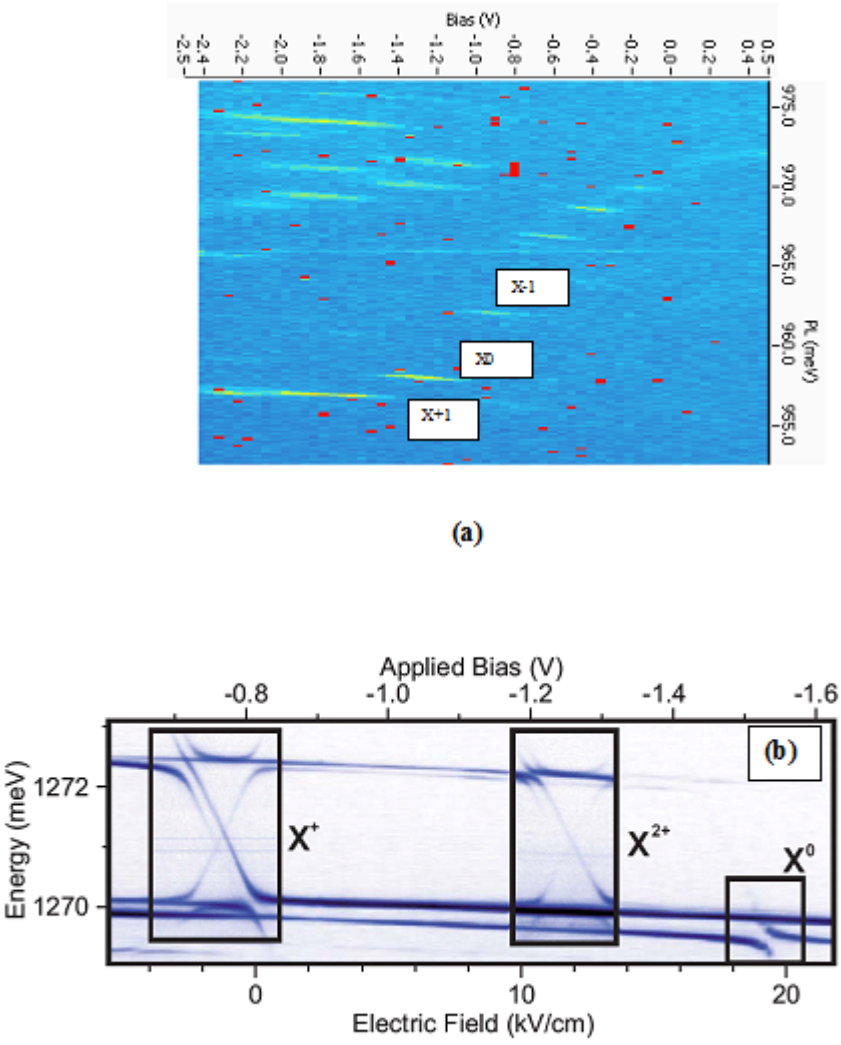

Figure 2.9: Comparison of electric field dependent PL recorded from a single InGaAs QD as a function of charge state (a) and an individual QDM (b) [4]. Fine structure of molecular resonances in the PL transitions of the neutral exciton (X0), positive trion (X+), and doubly positively charged exciton (X2+) in a QDM. Intensity of the PL line corresponds to more blue color

Vertically stacked QDMs provide an important test-bed for studying the interactions between spin localized in each dot because the thickness of the tunneling barrier between the dots can be precisely controlled with growth parameters. However, the vertically stacked geometry has severe scalability limitations. First, one can't make electrical contact to a series of dots all spaced vertically by a few nm. Second, the vertically-stacked geometry does not permit independent tuning of the charge state and the relative energy levels. Thus it is hard to simultaneously achieve both the desired charge state and the desired detuning and molecular state.. Consequently, we focus here on exploring the mechanisms and signatures of spin interactions in laterally separated QDMs. Laterally separated QDMs may enable a natural up-scaling to very large number of quantum gates across a semiconductor substrate [16] and independent control over both coupling and charge occupancy.

2.3 Lateral Quantum Dot Molecules

In this work we focus on developing methods to characterize the spin and charge interactions in laterally-coupled pairs of quantum dots. The fabrication of Lateral Quantum Dot Molecules (QDMs) is achieved by application of a shallow GaAs layer after the nucleation of InAs QDs. The original dome shape of the InAs is maintained during GaAs capping at below 360C. At temperatures between 400C-500C, the QDs go through a significant shape transition and can evolve into vari-

ous nanostructures. The shape evolutions are mainly driven by diffusion process induced by redistribution of the surface chemical potential and strain matrix [17]

Our samples were grown on semi-insulating GaAs (100) substrate using MBE by Jihoon Lee and G. J. Salamo, University of Arkansas. As_2 was used as an arsenic source throughout the whole growth procedure. Starting with a bare GaAs substrate, the native Ga oxide was desorbed by annealing the substrate at 600C for 10min. Then a 500nm GaAs buffer layer was grown at 610C at a growth rate of 0.75 monolayer per second (ML/s). To stabilize the surface the sample was post annealed at the same temperature. Then, at the growth rate of 1.65 ML/s, InAs QDs were grown at 520C. On these InAs QDs, at the surface temperature of 480C, 10ML of GaAs was applied which induced diffusion of the InAs to form Lateral QDMs as shown in figure 2.10.

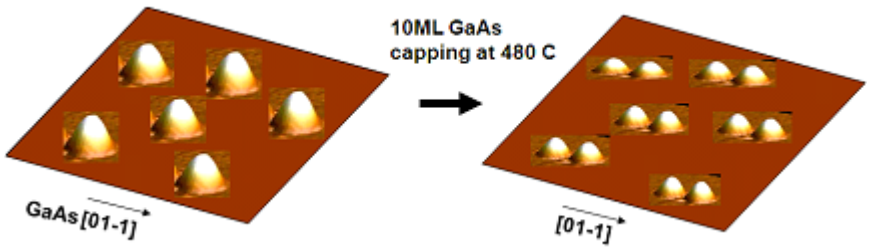

Figure 2.10: Growth Procedure of Lateral QDMs

These QDMs are elongated along the [01-1] direction, probably due to the anisotropic nature of the diffusion process on the GaAs surface. The GaAs sur-

face possesses reconstructed dimer-rows running along [01-1] with a (2 x 4) reconstruction [18, 19, 20, 21, 22, 23, 24] which favors atomic diffusion prefentially along [01-1], with a much weaker diffusion along [011].

Because the QDs are separated laterally, tuning the relative energy levels of the two dots requires a lateral electric field. To study the quantum mechanical coupling mechanisms and spin interactions in lateral QDMs, I used interdigitated electrodes patterned onto the sample surface with optical lithography and electron-beam metal deposition. The recipe for the optical lithography to achieve 1um critical dimension and e-beam deposition is described in Appendix.

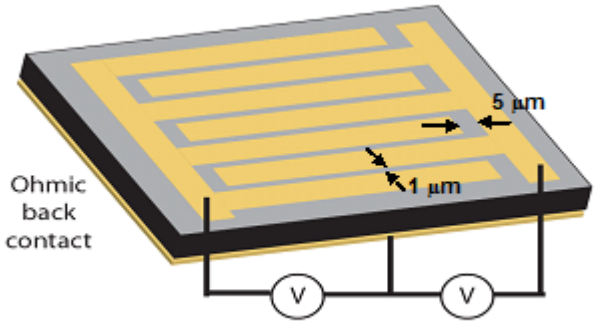

Figure 2.11: Inter-digitated electrodes for studying lateral QDMs

By choosing wide electrodes spaced by approximately 1 μ m, these electrodes can simultaneously serve as a shadow mask to isolate pairs of QDs along one dimension. This three terminal arrangement makes it possible to independently control both the relative energies of the two dots (with the two groups of interdig-

itated electrodes) and the charging of the dots (with the relative voltage between the top electrode and the back contact).

Chapter 3

Experimental Analysis of Quantum Dot Molecules

3.1 Time Integrated Photoluminescence (PL)

The quantum-dot structures discussed in the previous sections have been characterized by Photoluminescence (PL) spectroscopy. Time integrated photoluminescence spectroscopy (PL) is an important contact-less and non destructive characterization method, generally used to experimentally determine the electronic structure of semiconductor materials. The experimental setup and the results of these experiments are described here.

The principle of photoluminescence measurements is to create carriers by optical excitation with photon energy above the bandgap of the quantum structure.

Electrons and holes relax to their respective ground states in the conduction and valence band. The emission of light from a semiconductor is the result of the recombination of electrons and holes. The wavelength of the light is determined by the minimum energy difference between the recombining electron and hole states, as represented schematically in Fig. 3.1

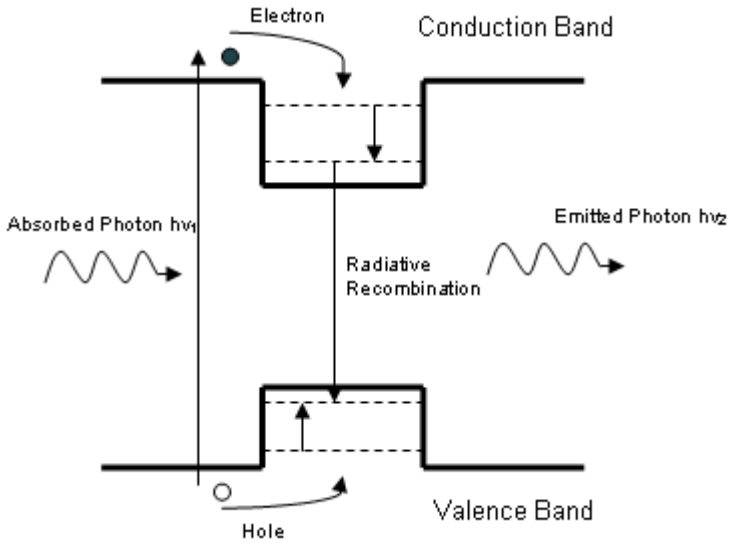

Figure 3.1: Optical emission and absorption in QD

The process of photoluminescence, represented schematically in Fig. 3.1, starts with the absorption of a photon from the exciting light source, usually a laser. The excitation photon creates an electron-hole pair in the bulk material. The charge carriers move by diffusion and are finally captured in the potential well created by a quantum dot, where they relax to the lowest energy states of the QDs and recombine by emitting a photon.

Photons generated only from the recombination in the ground state of the structure are detected because the recombination is a slower process than the relaxation. The energy levels of the QDs are determined by measuring the peak energy of the emitted photons. If the excitation intensity of the laser produces more carriers than the ground states can accommodate, emission from excited states can be observed. We examined the PL spectra recorded using both low and high laser intensities (excitation-dependent PL) at low temperature. At low intensities, not enough electron-hole pairs were generated to fill the ground states of the dots. At high excitation intensities, the number of carriers generated saturates the ground state, leading to emission from higher energy excited states. More detailed analysis of the electronic structure is possible if the PL emission from excited states is also measured.

3.2 Experimental set-up for PL

PL experiments were done using the 532 nm line of a Verdi V5 laser to pump Coherent Mira Ti:Sapphire laser which lases from 700-950nm wavelength and excites the PL. The laser beam diameter is 2.25 mm with a variable output power from 100mW to 800mW. The PL signal was collected by a Mitutoyo objective with high NA and optimized for NIR and analyzed using a 0.75m SpectraPro 2750 spectrometer equipped with an optical interface specially designed to max-

imize the collection efficiency. The samples were mounted on the cold finger of Advanced Research Systems (ARS) DMX-20 closed-cycle cryostat. The PL signal was detected using a liquid nitrogen cooled CCD detector. Fig 3.2 shows the PL experimental set-up.

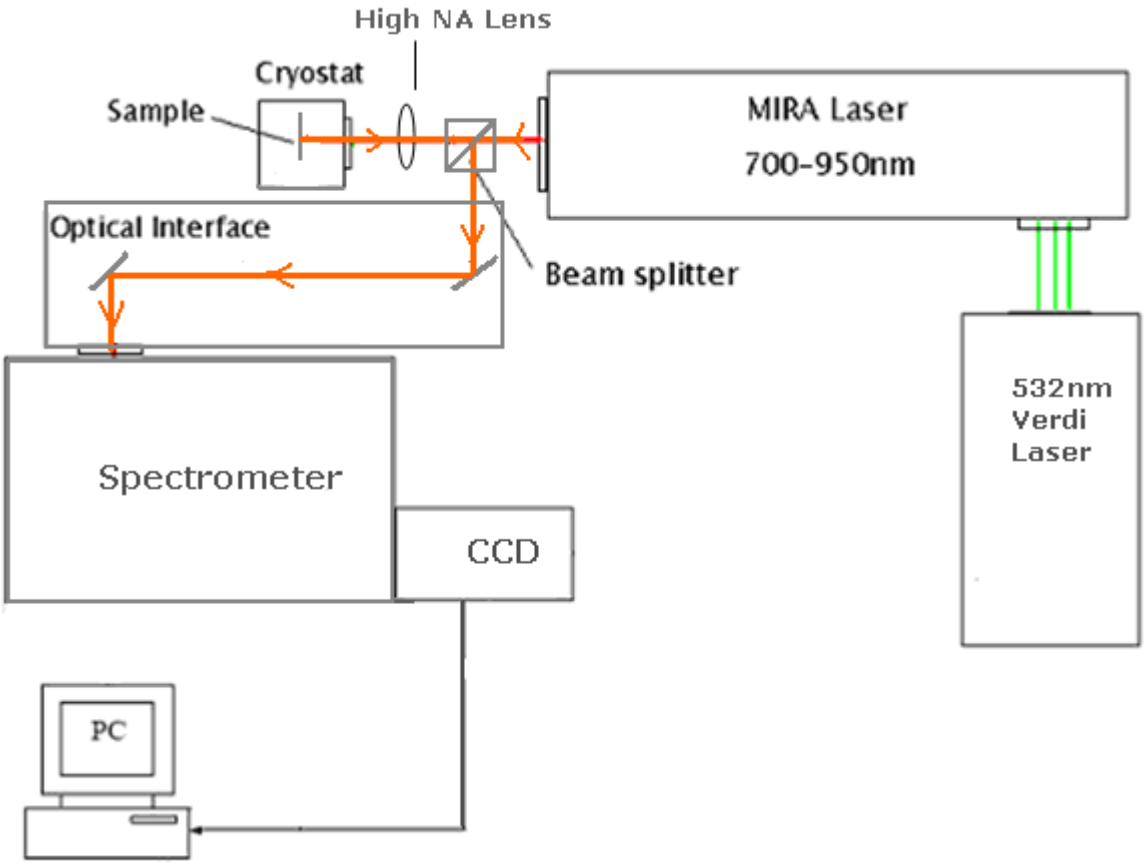

Figure 3.2: Schematic of the Photoluminescence experimental setup

Laser beam is passed to the experiment using mirrors and sent to a microscope objective using a beam splitter cube. The laser was focused onto the sample by using an anti-reflection coated convex M Plan Apo NIR High Resolution lens with 0.65 Numerical Aperture, 50 X magnification, 10mm working distance and 4mm focal length. The closed cycle cryostat ARS DMX-20 uses a mechanical refrigerator to reach the cryogenic temperature range without the of liquid helium which is expensive. The ARS closed cycle cryostat uses an internal pressure differential to move the displacer instead of a mechanical piston.

The refrigeration cycle of the ARS closed cycle cryostat starts with the rotation of the valve disk opening the high pressure path allowing the high pressure helium gas to pass through the regenerating material into the expansion space. Second, the pressure differential drives the piston "up" allowing the gas at the bottom to expand and cool. Third the rotation of the valve disk opens the low pressure path allowing the cold gas to flow through the regenerating material removing heat from the system. Finally the pressure differential returns the displacer to its original position completing the cycle. The expander with the valve motor is isolated from the sample mount via an isolation bellows to minimize the vibrations resulting from the movement of displacer.

The cryostat was cooled to a temperature of 8K. The cold finger of the cryostat was configured with a silicon diode to measure temperature and a wire round 25 Ω heater which can be used to stabilize the temperature. The heater and diode were

connected to a Lakeshore 331 temperature controller.

The SpectraPro 2750 spectrometer is completely computer controlled through a Lab View data acquisition board. The spectrometer is equipped with three reflective holographic diffraction gratings blazed at 800 nm, 1μm and H-NIR with a groove density of 150 g/mm, 600 g/mm and 1100 g/mm respectively. All experiments were completed with the diffraction grating with 1100 g/mm. The entrance slit width of the spectrometer was kept at 50μm throughout the experiments. The spectral resolution of our experimental set-up was 70 μeV.

Upon entering the spectrometer, the PL signal was collected by a collimating mirror that reflects the signal onto a reflective grating which disperses the component wavelengths of the PL signal onto a focusing mirror. The dispersed signal was detected by a liquid nitrogen cooled detector. A PL spectrum was plotted against energy using Labview software. PL spectra was acquired at sequential values of applied electric field and assembled to make a spectral map of PL intensities as a function of both applied electric field and energy. The data was then saved, organized, and processed using Origin software.

3.3 Experimental Data

The study of coupling in single QDs and vertically stacked QDMs is presented briefly. The results and limitations of these studies motivated the study of the

mechanisms of spin interactions in Lateral coupled QDMs. Figure 3.3 shows a spectral map of PL intensities as a function of both applied electric field and energy for single InGaAs QDs at 8K for laser excitation power density 20 W/cm^2 and laser wavelength of 870nm. Although the calculation of the absolute power density could be off by a factor of 4 or more, the relative changes in power density are accurate to a few percent. The applied bias voltage is varied from 0 to -2.5V and the spectrum is collected for PL energy ranging from 1280 meV to 1300 meV for an integration time of 30sec.

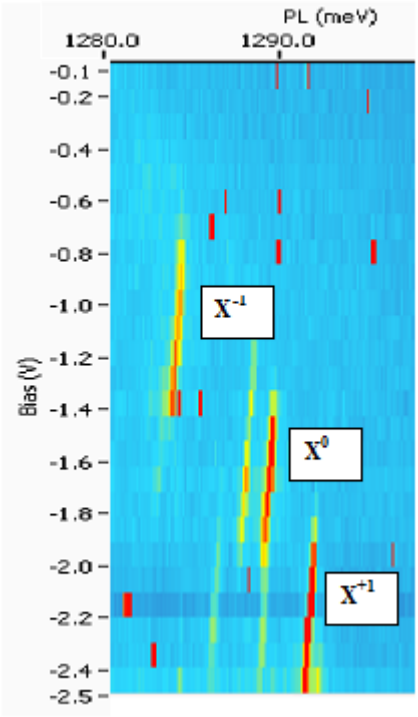

Figure 3.3: Spectral map for a Single InGaAs QDs. Intensity of the PL line corresponds to more red color than blue color

At the most negative applied voltage, we observe a spectral line for X+1 (positive trion) at energy of 1290.53 meV. An X+1 (positive trion) is generated by optical charging in which the electron tunnels out of the dot with the applied electric field, leaving behind a hole. The injected exciton recombines in the presence of this extra hole and results in an X+1(positive trion). At around -2V this X+1 (positive trion) starts overlapping with X0 (neutral exciton) and results into a spectral line for X0 at 1288.28 meV of energy. At -1.4V the X0 disappears and a new

line 5.27 meV lower show up, this spectral line is assigned to the X-1(negative trion). This energy shift is characteristic of the appearance of the negative trion (X-1) below the neutral exciton and is in agreement with the characteristics of self assembled InGaAs QDs [25]. This characteristic energy shift aids in the assignment of the lines to specific excitonic species. A negative trion at discrete bias voltage arises because the dot level crosses the Fermi level set by the substrate doping and therefore a single electron deterministically tunnels into the dot. The injected exciton recombines in the presence of this electron. The presence of these extra charges introduces Coulomb shifts to the energy.

Figure 3.4 shows a spectral map for InGaAs vertically stacked QDMs at 9K for laser excitation power density 600 W/cm^2 for laser wavelength 892nm. The applied bias voltage is varied from 1.1 V to 1.5 V and the spectrum is collected for PL energy ranging from 1318 meV to 1335 meV for an integration time of 120sec.

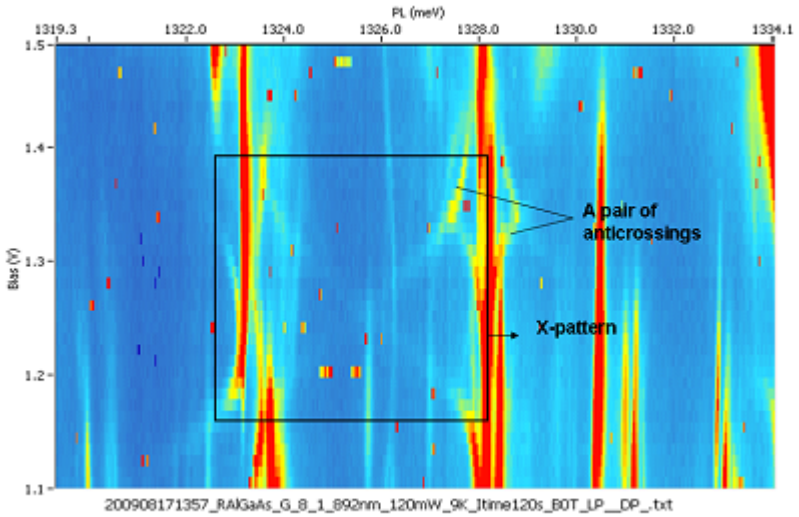

Figure 3.4: Spectral map for a vertically stacked InGaAs QDMs

In this spectral map we observe several anticrossings and indirect PL lines, indicative of tunnel coupling. They collectively give rise to an x-shaped pattern that is indicative of tunnel coupling in a charged exciton state. We are not able to spectrally resolve the splitting of anticrossings and different charged states. The anticrossings and indirect lines in this sample are relatively weak because of the presence of AlGaAs in the barrier layer as shown in figure 3.5

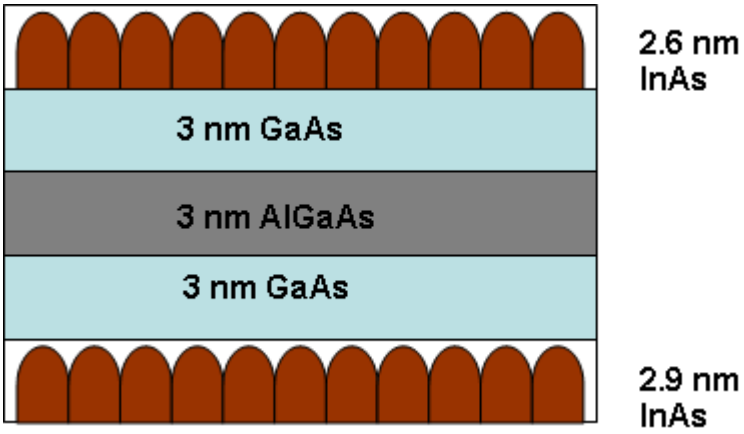

Figure 3.5: Schematic of Vertically aligned QDM sample

The valence and/or conduction band mismatch between AlGaAs and InAs is larger than that between GaAs and InAs. Consequently, the presence of the AlGaAs causes a higher potential in the barrier and reduces the probability of charge tunneling through the barrier. The higher barrier potential also reduces the overlap of the wavefuntions of electrons and holes in different dots, reducing the optical intensity of the photoluminescence from this indirect exciton. That's why the diagonal part in the anticrossings is not as clearly observed as in the original GaAs barrier samples cited in the literature [25, 14].

As the vertically stacked geometry has a severe scalability limitation and it does not permit independent tuning of the charge state and the relative energy levels, we proceed to studying Lateral QDMs. The electrode patterns on the surface of Lateral QDMs have different regions with apertures of width 5μ m and 1μ m (see figure 2.11).

Figure 3.6 illustrates the PL spectra observed from a 5μ m gap of electrodes in Lateral QDM. There are many dots in 5μm region, so we expect to see ensemble PL. The sample is held at 11 K and illuminated with excitation power densities ranging from 10 W/cm^2 to 75 W/cm^2. The spectra are taken at laser wavelength 780nm and for integration time 1 sec.

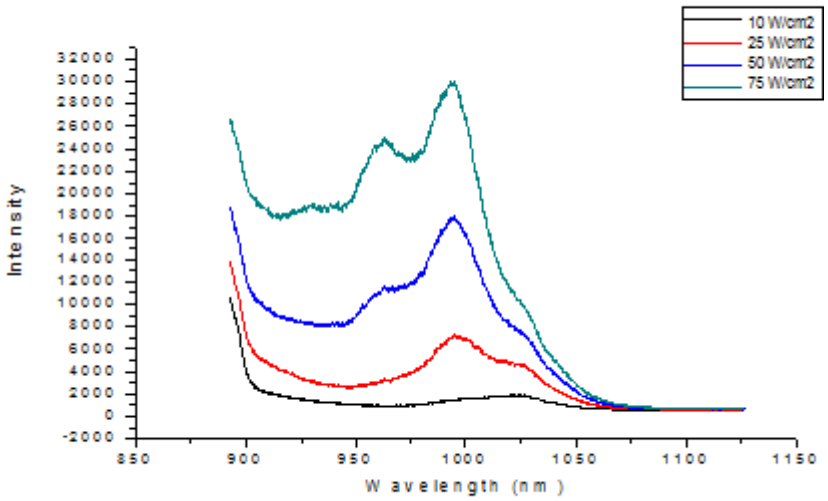

Figure 3.6: Excitation dependent PL spectra for Lateral QDMs

This PL spectrum is analyzed with the spectrometer diffraction grating of 1100 g/mm and at wavelengths above 900nm. In this spectral region we observe peaks only from the confined energy levels of QDs and not from the InAs wetting layer, which is characteristically around 860nm. It can be seen that the PL peak intensity increases with increasing the excitation power density, as more quantum dots con-

tribute to the PL emission. Also, at higher excitation power densities, the number of features in the spectra increases, as optical recombination from higher energy states begins to contribute to the PL signal. This is due to the saturation of lower energy states: when electron hole pairs are injected more rapidly than they can recombine from the ground state, the higher energy confined states begin to be filled and to emit PL.

To study spin and charge interactions (which are of the order of 1meV in energy) we proceed to look at QDMs in the region of the 1 μm gap. The 1μm gap serves as an effective aperture; on average a single dot lies within the region defined by the 1μm gap and the focal spot of our microscope objective (5μm diameter). The PL line spectrum for a single Lateral QDM is shown in figure 3.7. This PL spectrum is obtained at 11K for laser excitation power density 250 W/cm^2 and laser wavelength of 870nm with -1V applied bias voltage for an integration time of 10sec.

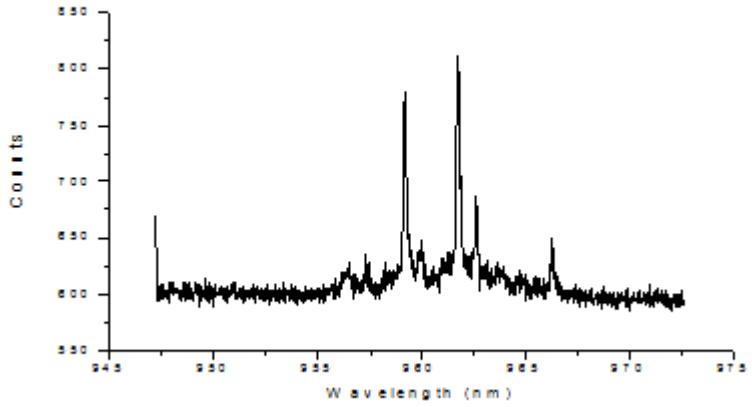

Figure 3.7: PL spectra for a single Lateral QDMs

The spectra of Fig 3.7 show a few distinct peaks separated by few meV in energy. This line spectrum confirms that we are successfully able to isolate a single QDM in this lateral geometry using our 3 terminal electrode design. We observe two strong peaks and 4 other weak peaks in this PL spectrum. In order to assign the lines to specific charge states and to study the presence of tunnel coupling, we apply the electric field.

Figure 3.8 (b) shows a spectral map of PL intensities as a function of both applied voltage and energy for laterally spaced InGaAs QDM. First we apply electric field between top and bottom contact of the Schottky diode structured sample with the two top electrodes tied to each other as shown in figure 3.8 (a).

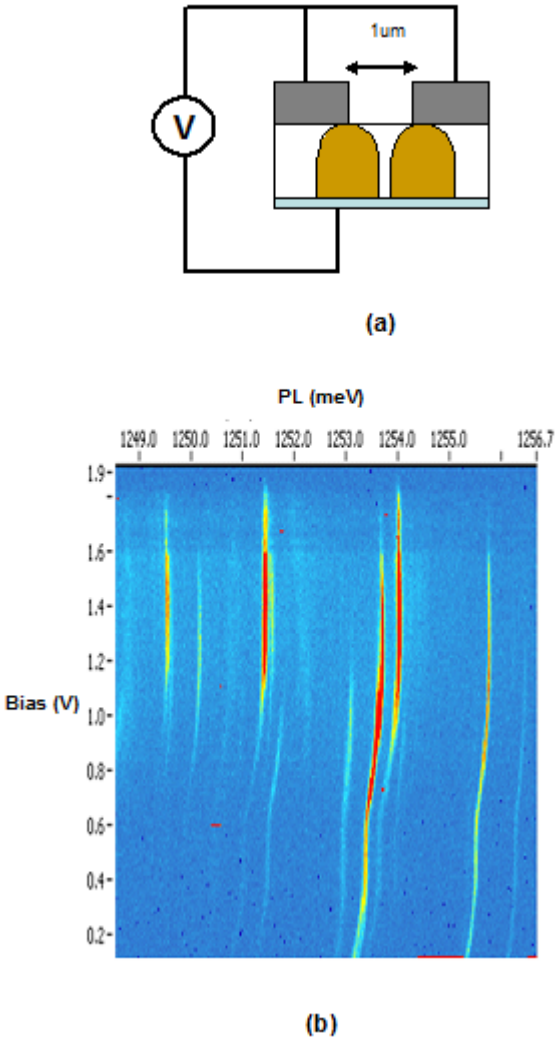

Figure 3.8: (a) Schematic of the voltage applied between the top electrodes and the back contact (b) Spectral map for InGaAs QDMs with one applied voltage

The PL spectral map shown in figure 3.8 (b) is obtained at 12K for laser excitation power density 40 W/cm^2 and laser wavelength of 870nm. The applied bias voltage is varied from 0 to 2.0V and the spectrum is collected for PL energy ranging from 1248 meV to 1257 meV for an integration time of 5sec. In the figure 3.8 (b) a pair of PL lines are seen, which are less than 0.5meV apart in energy. This pair of lines is suggestive of Coulomb interactions in QDMs, which are well understood in vertically stacked QDMs. The presence of an additional charge in the second dot induces a small energy shift to the exciton in the first dot, giving rise to a PL doublet [14]. We stress, however, that the assignment of lines for these lateral QDMs is extremely tentative. Recent results suggest that complex exciton formation dynamics may influence the observed excitonic lines [26].

Next we tune the relative energies of the dots with a second bias voltage applied between the two parallel electrodes, which provide a lateral electric field perpendicular to the molecular axis. A schematic of applied voltages V1, between the back contact (substrate) and 1 top electrode and V2, which applies the lateral electric field between the two top electrodes, is shown in figure 3.9 (a). Figure 3.9 (b) shows a PL spectral map at 12K for laser excitation power density 40 W/cm^2 and laser wavelength of 870nm. V1 is fixed at 1.4V and V2 is varied from -0.3V to 1.5V. The spectrum is collected for PL energy ranging from 1250 meV to 1257 meV for an integration time of 30sec.

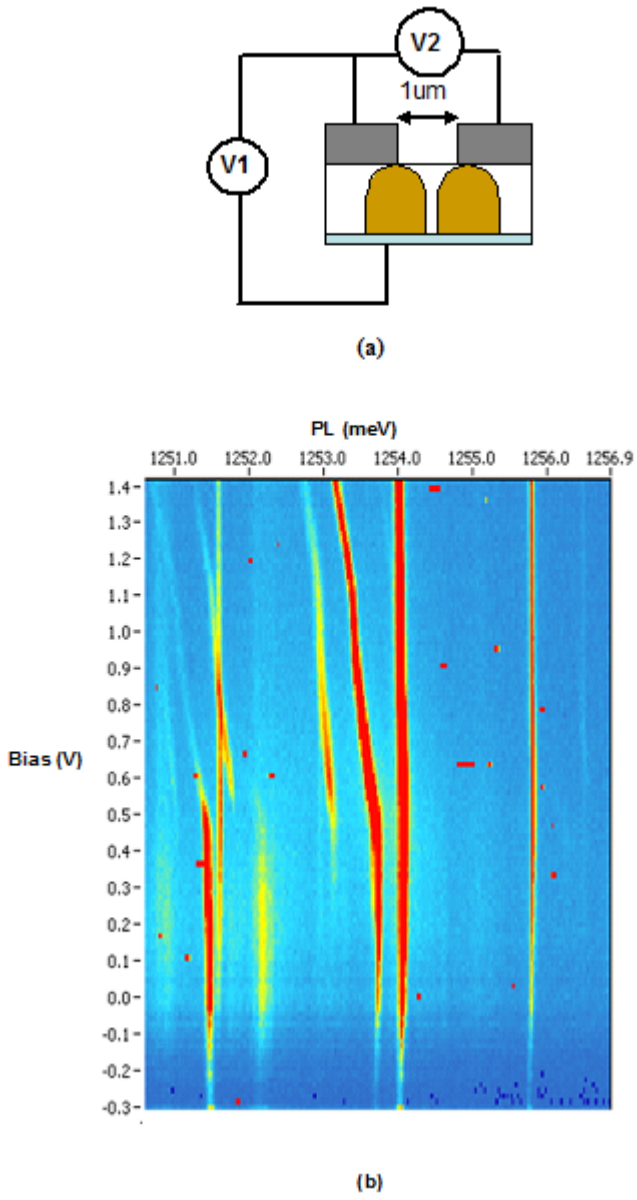

Figure 3.9: (a) Schematic of the voltage applied between the top electrodes and the back contact (b) Spectral map for InGaAs QDMs with one applied voltage

A PL spectral line at 1254meV does not have an energy dependence on the applied electric field. Another very strong PL line (at 1253.3 meV at 1.4 mV) is seen to have a strong dependence of energy on applied electric field. By comparison with findings of vertical geometry of QDMs [14], these two lines are suggestive of direct and indirect excitons. The proximity of the two lines at a bias voltage of 0.3V is suggestive of an anticrossing, though the lines do not diverge symmetrically on opposite sides of the anticrossing point. Recent work suggests that the direct observation of anticrossings in lateral QDMs may be suppressed by the Coulomb interactions between electrons and holes [26].

3.4 Discussions and Future Work

We have investigated the optical properties of InGaAs Lateral QDM structures. Optical spectra of the QDMs as a function of vertical and lateral electric field are presented. These spectra provide preliminary indications of coupling between the two dots. To prepare these samples we have developed fabrication techniques to deposit interdigitated electrodes which allow us to simultaneously probe single QDMs and tune the coupling between the two dots. Integration of such devices on periodically arranged QDMs could lead to deterministically controlled devices based on QDMs, but further exploration of the mechanisms of coupling and their dependence on applied electric field and QDM structure are necessary.

Future work will focus on developing a deeper understanding of the coupling between the two dots in Lateral QDMs. Areas of investigation will include charge carrier dynamics, excitonic polarization, and magnetic field effects. Charge carrier dynamics will look at the radiative lifetime of each line to determine relaxation processes, which can provide information on the dynamic motion of carriers into and between the dots. For the real devices, the dynamics of the recombination is of the utmost importance because it limits the maximum modulation frequency of the device and the coherence time of the emitted light [27].

Studying the excitonic polarization will allow in identifying different excitonic charge states and will provide an optical photoluminescence excitation (PLE) method to selectively probe the spin state of a single electron confined in a QD [28, 29].

Magneto-optical experiments can provide additional insight into the mechanism of quantum coupling in these QDMs. In vertical QDMs, magneto-optical experiments revealed tunable g factors that could provide new tools for manipulating spins by tuning spin splitting into resonance with external AC magnetic fields or by using g tensor modulation [28, 30]. Moreover, the resonant changes in g factor permitted identification of the orbital character of delocalized states and detection of a surprising reversal of the symmetry of the orbital character of the molecular ground state [31]. Similar effects are anticipated for lateral QDMs, which could provide insight into the molecular character of delocalized states.

Appendix A

Sample Preparation with Optical Lithography and e-beam metal deposition

1. Cleaning Step - Mount wafer on spinner. Spin at 3000 rpm/s and ramp 1000 rpm/s for 45 sec. Start cleaning as:
   - Spray Acetone for 10 sec
   - Spray Methanol for 10sec
   - Spray Iso-propanol for 10sec
2. Resist
   - Drip on Shipley-1813 photoresist until covers the surface of the sample

- Spin at 5000 rpm/s , ramp 1000 rpm/s for 40sec
- Bake at 115degC for 1min

3. Edge bead Exposure and Development
   - Expose perimeter of the chip to UV for 20sec
   - Develop in MF-321 for 5sec (with shaking the sample in the developer)
   - Rinse in DI-water
   - Gently blow dry with nitrogen
4. Pattern Exposure and Development
   - Expose pattern for 20sec
5. Toluene Treatment
   - Dip the sample in Toluene for 75sec in a beaker
   - Blow dry
   - Hard bake for 20sec at 90degC
6. Developing Step
   - Develop in MF-319 for 5sec (with shaking the sample in the developer)
   - Rinse in DI-water and dry with nitrogen blow
   - Check the pattern and additional dips in MF-319 if necessary

For the ohmic back contact Ni, Au, Ge are deposited using e-beam evaporator in the following order followed by a 30 sec annealing in Rapid Thermal Annealer (RTA) at 410degC.

S.No.	Material	Thickness (nm)
1.	Ni	5
2.	Ge	17
3.	Au	33
4.	Ni	15
5.	Au	20

Table A.1: Position Order and thicknesses of materials used for ohmic back contact

A 50 A layer of Ti followed by 1300 A layer of Al was deposited on the top surface of the sample. Thus by choosing these electrodes spaced by 1m, they serve as a shadow mask to isolate pairs of QDs along one dimension.

Bibliography

[1] Miro Kroutvar, Yann Ducommun, Dominik Heiss, Max Bichler, Dieter Schuh, Gerhard Abstreiter, Jonathan J. Finley, Nature 432, 81-84 (2004)

[2] "Spin Electronics", edited by David D. Awschalom, Robert A. Buhrman, James M. Daughton, Stephan von Molnar and Michael L. Roukes

[3] wikipedia.com

[4] Guido Burkard, Nature Materials, Vol. 7, February 2008

[5] Y. Ducommuna, M. Kroutvara, J.J. Finleya, M. Bichlera, A. Zrennerb, G. Abstreitera, Physica E 21 (2004) 886 - 891

[6] "Semiconductor Spintronics and Quantum Computation" by D. D. Awschalom, D. Loss and N. Samarth

[7] S. Amasha, K. MacLean, Iuliana P. Radu, D. M. Zumbu¨hl, M. A. Kastner, M. P. Hanson, and A. C. Gossard, Phys. Rev. Lett. 100, 046803 (2008)

[8] J.I. Cirac and P. Zoller, Phys. Rev. Lett. 74, 20 (1995)

[9] Daniel Loss and David P. DiVincenzo, Phys. Rev. Lett. A 57, 1 (1998)

[10] L J Rogers, R L McMurtie, M J Sellars and N B Manson, New Journal of Physics 11 (2009) 063007

[11] M. Suguwara, "Self assembled InGaAs/GaAs quantum dots" (1999)

[12] H. Drexler, D. Leonard, W. Hansen, J.P. Kotthaus, and P.M. Petroff, "Spectroscopy of Quantum Levels in Charge-Tunable InGaAs Quantum Dots," Phys. Rev. Lett. 73, 2252 (1994)

[13] M. Baier, F. Findeis, A. Zrenner, M. Bichler, and G. Abstreiter, "Optical spectroscopy of charged excitons in single quantum dot photodiodes,"Phys. Rev. Lett. B 64, 195326 (2001)

[14] M. Scheibner, M. F. Doty, I. V. Ponomarev, A. S. Bracker, E. A. Stinaff, V. L. Korenev, T. L. Reinecke, and D. Gammon,Phys. Rev. Lett. B 75, 245318 (2007)

[15] A. S. Bracker, M. Scheibner, M. F. Doty, E. A. Stinaff, I. V. Ponomarev, J. C. Kim, L. J. Whitman, T. L. Reinecke, and D. Gammon ,Applied Physics Letters 89, 233220 (2006)

[16] G. J. Beirne, C. Hermannsta¨dter, L. Wang, A. Rastelli, O. G. Schmidt, and P. Michler, Phys. Rev. Lett. 96, 137401 (2006)

[17] J. H. Lee, Zh. M. Wang, Yu. Mazur, V. G. Dorogan, M. E. Ware and G. J. Salamo, IEEE Transactions on Nanotechnology, 8 (2009)

[18] P. Laukkanen, M. Kuzmin, R. E. Perala, M. Ahola, S. Mattila, I. J. Vayrynen, J. Sadowski, Phys. Rev. B, 72, 045321-9, 2005.

[19] L. Broekman, R. Leckey, J. Riley, B. Usher, B. Sexton,Surf. Sci.,331-333, 1115-21, 995

[20] D. W. Pashley, J. H. Neave, B. A. Joyce, Surf. Sci., 582, 189-201, 2005.

[21] D.K. Biegelsen, R.D. Bringans, J. E. Northrup, L. -E. Swartz, Phys. Rev. B, 41, 5701-6, 1990.

[22] J. H. Lee, Zh. M. Wang, W. T. Black, Vas. P. Kunets, Yu. I. Mazur, and G. J. Salamo, Adv. Funct. Mater, 17, 3187-3193, 2007.

[23] J. H. Lee, Zh. M. Wang, N. W. Strom, Yu. I. Mazur and G. J. Salamo, Appl. Phys. Lett., 89, 202101-3, 2006.

[24] Zh M Wang, J. H. Lee, B L Liang, W T Black, Vas P Kunets, Yu I Mazur, and G J Salamo, Appl. Phys. Lett., 88, 233102, 2006.

[25] H.J. Krenner, E.C. Clark, T. Nakaoka, M. Bichler, C. Scheurer, G. Abstreiter, and J.J. Finley, Phys. Rev. Lett. 97, 076403 (2006)

[26] J. Peng, C. Hermannstädter, M. Witzany, M. Heldmaier, L. Wang, S. Kiravittaya, A. Rastelli, O. G. Schmidt, P. Michler and G. Bester, Mesoscale and Nanoscale Physics, (2009)

[27] M. Feucker, R. Seguin, S. Rodt, A. Hoffmann, and D. Bimberg, Appl. Phys. Lett. 92, 063116 (2008)

[28] M. E. Ware, E. A. Stinaff, D. Gammon, M. F. Doty, A. S. Bracker, D. Gershoni, V. L. Korenev, ?. C. B?descu, Y. Lyanda-Geller, and T. L. Reinecke, Phys. Rev. Lett. 95, 177403 (2005)

[29] C. Hermannstädter, M. Witzany, G. J. Beirne, W.-M. Schulz, M. Eichfelder, R. Rossbach, M. Jetter, P. Michler, L. Wang, A. Rastelli, and O. G. Schmidt, Journal of Applied Physics 105, 122408 (2009)

[30] Y. Kato, R. C. Myers, D. C. Driscoll, A. C. Gossard, J. Levy, and D. D. Awschalom, Science 299 1201-1204 (2003)

[31] M. F. Doty, J. I. Climente, M. Korkusinski, M. Scheibner, A. S. Bracker, P. Hawrylak, and D. Gammon, Phys. Rev. Lett. 102, 047401 (2009)